Acta Pharmaceutica Sinica B 2025;15(10):5400−5415

Chinese Pharmaceutical Association
Institute of Materia Medica, Chinese Academy of Medical Sciences

Acta Pharmaceutica Sinica B

www.elsevier.com/locate/apsb
www.sciencedirect.com

ORIGINAL ARTICLE

Cerium single-atom catalysts-armed *Lactobacillus reuteri* for multipronged anti-inflammatory/anti-fibrotic therapy of inflammatory bowel disease

Yinying Pu[a], Shaorong Huang[b], Shuang Gao[c], Yangying Duan[a], Wenhao Li[a], Qiyue Li[a], Han Lin[d], Kun Zhang[a,*], Min Zhou[c,*], Wencheng Wu[a,*]

[a]*Central Laboratory and Department of Medical Ultrasound, Sichuan Academy of Medical Sciences, Sichuan Provincial People's Hospital, University of Electronic Science and Technology of China, Chengdu 610072, China*
[b]*Institute of Geriatrics, Jiangxi Provincial People's Hospital, the First Affiliated Hospital of Nanchang Medical College, Nanchang 330006, China*
[c]*Digestive Endoscopy Center, Shanghai Fourth People's Hospital to Tongji University, Shanghai 200081, China*
[d]*Shanghai Institute of Ceramics, Chinese Academy of Sciences, Shanghai 200050, China*

Received 18 February 2025; received in revised form 7 April 2025; accepted 20 May 2025

KEY WORDS

Antioxidant therapy;
Catalytic;
Cerium single-atom catalyst;
Gut microbiota;
Intestinal fibrosis;
Inflammatory bowel disease;
Probiotic;
Reactive oxygen radicals

Abstract Simultaneous management of intestinal mucosal barrier dysfunction and gut microbiota dysregulation represents a significant challenge in the treatment of inflammatory bowel disease (IBD). Herein, we report a novel system that integrates multi-enzyme mimicking cerium single-atom nanocatalysts (CeSACs) with *Lactobacillus reuteri* probiotics (LR@CeSACs) for multipronged management of IBD. In this system, CeSACs demonstrate robust multi-enzyme activities across a broad pH range, effectively scavenging elevated reactive oxygen species, downregulating pro-inflammatory cytokines, and suppressing the expression of fibrosis-related genes. Moreover, probiotics promote the targeting and retention of the CeSACs for sustained catalytic antioxidant therapy. In turn, the inflammation relief enabled by CeSACs promotes bacterial viability, allowing for the rapid reshaping of intestinal barrier function and the restoration of gut microbiota. Therefore, LR@CeSACs exhibit excellent catalytic anti-inflammatory and anti-fibrotic therapeutic effects, as well as a certain prophylactic effect, as demonstrated in several murine models.

*Corresponding authors.
E-mail addresses: wuwencheng@uestc.edu.cn (Wencheng Wu), crown_zhou@hotmail.com (Min Zhou), zhang1986kun@126.com (Kun Zhang).
Peer review under the responsibility of Chinese Pharmaceutical Association and Institute of Materia Medica, Chinese Academy of Medical Sciences.

https://doi.org/10.1016/j.apsb.2025.06.022

1. Introduction

Inflammatory bowel disease (IBD), including idiopathic conditions like Crohn's disease and ulcerative colitis, significantly burdens patients and society[1-3]. Moreover, intestinal fibrosis induced by IBD can cause the narrowing of specific segments of the intestine, significantly disrupting its structure and function and ultimately increasing the risk of colorectal cancer[4]. Although the pathogenesis of IBD remains unclear, accumulating evidence suggests that it may be attributed to chronic relapsing inflammation of the gastrointestinal tract and gut microbiota dysregulation[5-7]. This dysregulation subsequently triggers a hyperactive immune response marked by increased reactive oxygen species (ROS) and inflammatory factors[8-10]. To alleviate intestinal inflammation, current therapeutic strategies predominantly involve the use of aminosalicylates, corticosteroids, immunomodulators, and biologics[11,12]. Nevertheless, a substantial proportion of patients did not derive benefit from these treatments. Furthermore, the prolonged use of these conventional drugs is associated with significant adverse effects over time, including immunosuppression, ecological disturbances, opportunistic infections, and organ damage[13]. These adverse effects stem from the irreversible depletion, rapid metabolism, and non-selective interactions of the drugs. Consequently, developing new pharmacological agents is crucial to overcoming these limitations and enhancing patient outcomes.

Recently, a diverse array of nanocatalysts exhibiting antioxidant and anti-inflammatory properties has been developed[14-17]. Notable examples, including CeO_2, Pt@PCN222-Mn, $LiMn_2O_4$, and $Cu_{5.4}O$, have demonstrated the ability to mimic various natural antioxidants and have shown therapeutic potential against IBD[18-21]. In particular, single-atom nanocatalysts have garnered significant attention due to their high atomic efficiency and superior catalytic activities[22]. These high-performance single-atom nanocatalysts have been extensively investigated for applications in electrochemical oxygen evolution, reduction reactions, photocatalytic energy conversion, and biomedical frontiers[23-25]. In contrast to traditional catalysts, single-atom nanocatalysts demonstrate the advantage of providing stable and sustained catalytic activity[26]. Nonetheless, the limited targeting and retention of these nanocatalysts at sites of inflammation present a significant challenge that restricts their application in the treatment of IBD. Consequently, given the therapeutic needs associated with IBD, single-atom nanocatalysts exhibiting high catalytic antioxidant activity are particularly promising, provided that the issue of intestinal targeting can be effectively addressed.

Oral probiotic therapeutics, using live bacterial cells, offer a promising intervention to restore gut microbiota dysregulation and repair intestinal mucosa[27,28]. Among the various probiotic strains, *Lactobacillus reuteri* (LR) is a well-established lactic acid bacterium that is naturally found in the intestinal tracts of nearly all vertebrates and mammals[29]. LR strongly adheres to the intestinal mucosa, enhancing microbiota distribution and inhibiting pathogenic colonization, thereby preventing intestinal diseases[30]. Consequently, oral administration of LR probiotics represents a safe and multifunctional therapeutic strategy for IBD. Nevertheless, the absence of antioxidant enzymes at the inflammation site renders these orally administered probiotics vulnerable to ROS attack[31]. This susceptibility diminishes their activity and colonization capacity, ultimately undermining therapeutic efficacy and extending the duration of treatment. It can be believed that advanced IBD therapeutic outcomes can be achieved by further integrating probiotics with antioxidant single-atom catalysts to simultaneously manage intestinal inflammation and gut microbiota dysregulation.

To fulfill the above demand, we established a novel single-atom nanocatalysts-armed LR probiotics suitable for oral administration, which can directly target the inflamed colon through the active chemotaxis of probiotics towards the infection for multi-pronged treatment of IBD. In this platform, the cerium single-atom catalysts (CeSACs) featuring atomically dispersed cerium active metal centers have been synthesized and utilized to effectively mimic natural antioxidant enzymes to not only replace traditional anti-inflammatory drugs but also shield probiotics from ROS stress (Fig. 1A). Specifically, CeSACs exhibit multi-enzyme mimetic properties, demonstrating both superoxide dismutase (SOD) and catalase (CAT)-like activities, along with hydroxyl radical scavenging capabilities. These properties make CeSACs efficiently and rapidly neutralize various ROS, down-regulate pro-inflammatory cytokines, as well as suppress fibrosis-related gene expression, thereby alleviating inflammatory symptoms. Furthermore, CeSACs protect encapsulated LR probiotics from oxidative damage within the inflamed environment, thereby facilitating the restoration of barrier function and promoting a beneficial state of the gut microbiota. In turn, the guarded LR probiotics offer health benefits to the host and exhibit strong intestinal colonization, ensuring prolonged antioxidant therapy of CeSACs in the site of infection (Fig. 1B and C). Thus, LR@CeSACs can mitigate ROS levels, inhibit proinflammatory cytokine secretion, suppress fibrosis-related gene expression, and restore gut microbiota balance, thereby providing comprehensive therapeutic effects for IBD. Notably, LR@CeSACs also exhibit a prophylactic effect against IBD in murine models.

2. Materials and methods

2.1. Materials

$Zn(NO_3)_2 \cdot 6H_2O$, $FeCl_3 \cdot 6H_2O$, $CeCl_3 \cdot 7H_2O$, 2-methylimidazole and 2,20-azinobis (3-ethylbenzthiazoline-6-sulfonate) (ABTS) were obtained from Aladdin Company. Other chemicals were provided by Beijing Chemical Works. Ultrapure water (Millipore, 18.23 MΩ cm) was used throughout all experiments. All the chemicals used in this experiment were analytical grade and used without further purification. 5,5-Dimethyl-1-pyrroline *N*-oxide (DMPO),2,2,6,6-tetramethylpiperidine-1-oxyl (TEMPO), superoxide dismutase (SOD), catalase, and glutaraldehyde fixative were obtained from Beyotime Biotechnology Co. High-purity $HClO_4$ and 5% (*w*/*w*) Nafion ionomers were purchased from Sigma (Shanghai, China). Silane-PEG-NH_2 was bought from Shanghai Yare Biotech, Co., Ltd. Simulated body fluid (SBF) solutions with

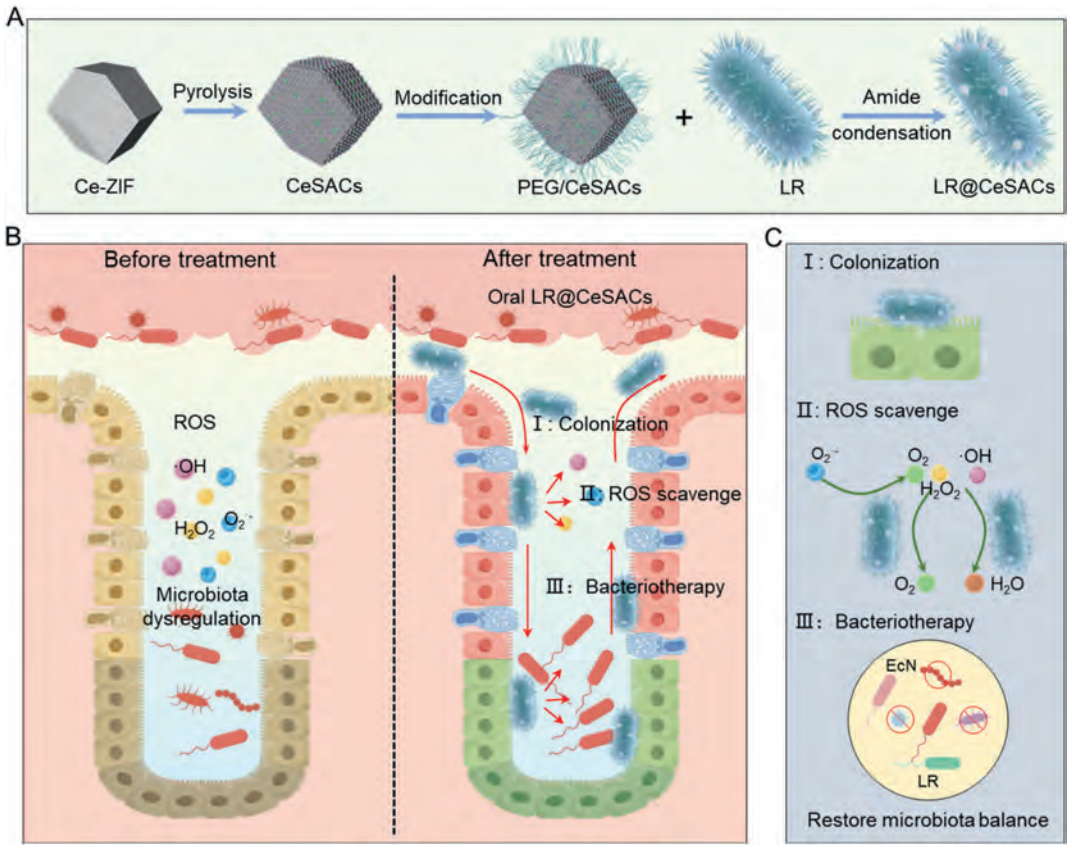

Figure 1 Schematic illustration of LR@CeSACs preparation and its mechanism for IBD treatment. (A) Preparation of CeSACs by pyrolysis of Ce-ZIF nanoparticles, modification of CeSACs with the NH_2-PEG-Silane, and conjugation of PEGlated CeSACs to the surface of LR. (B, C) LR endows LR@CeSACs with a strong colonization ability and extends the retention time of CeSACs in the intestine (I). Additionally, the prepared LR@CeSACs exhibit ROS-scavenging activity by mimicking various enzyme activities (II), thereby enhancing bacteriotherapy and restoring gut microbiome homeostasis (III).

different pH values were purchased from Dongguan Xinheng Technology Co., Ltd. RPMI-1640 (Roswell Park Memorial Institute), penicillin/streptomycin solution, and trypsin-ethylene diamine tetra-acetic acid (Trypsin−EDTA, 0.05%) were purchased from Gibco BRL (Gaithersburg, USA). Roswell Park Memorial Institute 1640 (RPMI 1640), phosphate-buffered saline (PBS), and dimethyl sulfoxide (DMSO) were purchased from Biosharp (Hefei, China). All reagents were used as received without further processing. Calcein, 4,6-diamidino-2-phenylindole (DAPI), propidium iodide (PI), fluorescein isothiocyanate (FITC), superior fetal bovine serum (sFBS, U11-020A), and cell counting kit-8 (CCK-8) were purchased from YOBIBIO (Shanghai, China).

2.2. *Synthesis of Ce@ZIF-8*

In summary, 0.325 g of 2-methylimidazole was dissolved in 40 mL of methanol. Subsequently, 20 mL of methanol containing 0.15 g of $Zn(NO_3)_2 \cdot 6H_2O$ and 14 mg of $CeCl_3 \cdot 7H_2O$ was added to the solution. The mixture was stirred at room temperature for 24 h. The resulting yellow crystals of Ce@ZIF-8 were isolated *via* centrifugation, washed with ethanol, and dried at 60 °C for 12 h.

2.3. *Preparation of Ce−N−C single atom catalysts (CeSACs)*

Initially, the Ce@ZIF-8 powder was subjected to thermal treatment in an argon atmosphere at 950 °C for 1 h, with a heating rate of 5 °C per minute, followed by natural cooling to room temperature. Subsequently, the carbonized material underwent etching with a 0.1 mol/L $HClO_4$ solution for 12 h to eliminate unstable metal species. The material was then filtered, thoroughly washed with deionized water, and dried for subsequent use.

2.4. *PEG modification of CeSACs*

Initially, 5 mg of CeSACs powder was dissolved in 10 mL of deionized water. Subsequently, 50 mg of Silane-PEG-NH_2 was added to the solution, which was then stirred in a water bath maintained at 60 °C for 12 h. The resultant mixture was collected by centrifugation and subjected to three successive washes with deionized water to yield PEGylated nanoparticles (PEG/CeSACs).

2.5. *Labelling of Cy5.5*

Initially, 1 mg EDS, 1 mg NHS, and 5 mg of PEG/CeSAs powder was dissolved in 10 mL of deionized water. Subsequently, 10 mg of Cy5.5 was added to the solution, which was then stirred in a water bath maintained at 60 °C for 12 h. The resultant mixture was collected by centrifugation and subjected to three successive washes with deionized water to obtain Cy5.5 labeled CeSACs.

2.6. Fabrication of CeSACs-armed LR probiotics

Lactobacillus reuteri (LR; ATCC 55148, a commercial probiotic strain; https://www.atcc.org/products/23272) was anaerobically cultured in a tube containing #1490 broth with shaking, or on a blood agar plate under static conditions, at 37 °C for 18 h. Subsequently, LR was harvested from the broth or plate, and its concentration was determined *via* plate counting. The resulting bacterial load (1×10^7 colony-forming units (CFU) per mL) was then incubated with CeSACs (50 μg/mL) under shaking conditions for 30 min to facilitate the assembly of CeSACs on LR through amino acid reactions. Finally, the synthesized LR@CeSACs can be either directly utilized or stored in an anaerobic tube containing the medium for extended periods at 4 °C. Additionally, LR@CeSACs with varying ratios were produced by altering the concentrations of LR and CeSACs.

2.7. XAFS measurements and data analysis

XAFS measurements at Ce L3-edge in both transmission and fluorescence (for samples) mode were performed at the BL14W1 in Shanghai Synchrotron Radiation Facility (SSRF). The electron beam energy was 3.5 GeV and the stored current was 230 mA (top-up). A 38-pole wiggler with a maximum magnetic field of 1.2 T inserted in the straight section of the storage ring was used. XAFS data were collected using a fixed-exit double crystal Si (111) monochromator. The photon flux at the sample position was 2.6×10^{12} photons per second. The raw data analysis was performed using IFEFFIT software package according to the standard data analysis procedures. The spectra were calibrated, averaged, pre-edge background subtracted, and post-edge normalized using Athena program in IFEFFIT software package. The Fourier transformation of the k2-weighted and k2-weighted EXAFS oscillations from k space to R space to obtain Fe K-edge and Ce L3-edge radial distribution function, respectively. Data fitting was done by Artemis program in IFEFFIT. Total electron yield (TEY) spectra of Fe L-edge and C/O K-edges were collected at the soft X-ray beamline BL08U1A at SSRF.

2.8. Bacterial viability under oxidative stress

Bacterial viability under oxidative stress was assessed by incubating native *Lactobacillus reuteri* (LR) at a concentration of 1×10^7 CFU/mL and LR encapsulated in CeSACs (LR@CeSACs) with varying feeding ratios in PBS buffer (pH 7.4, 10 mmol/L) containing 200 μmol/L H_2O_2 at 37 °C for 2 h. Subsequently, a 100 μL aliquot was collected from each tube, and bacterial counts were determined using blood agar plate counting methods.

2.9. In vitro ROS-scavenging activities of CeSACs

A SOD Assay Kit was employed to assess the superoxide anion ($O_2^{\cdot -}$) scavenging capacity of CeSACs. Initially, a dispersion of CeSACs was introduced into a working solution containing water-soluble tetrazolium salt (WST), which reacts with $O_2^{\cdot -}$. Subsequently, xanthine oxidase was added, and the mixture was thoroughly homogenized (the final germanium concentrations of CeSACs were 0, 5, 10, and 20 μg/mL). Following an incubation period of 20 min at 37 °C, the absorbance of the various solution groups was measured at a wavelength of 450 nm. Electron Spin Resonance (ESR) assay: The $O_2^{\cdot -}$ generated through the photolysis of riboflavin (50 μL, 6 mmol/L) served as a substrate to evaluate the scavenging efficacy of CeSACs. The spin-trap agent 5,5-dimethyl-1-pyrroline *N*-oxide (DMPO) was employed to capture $O_2^{\cdot -}$, forming the DMPO-$O_2^{\cdot -}$ adduct, which exhibited characteristic peaks in the ESR spectra. Variations in the intensity of these characteristic peaks were subsequently analyzed to determine the $O_2^{\cdot -}$ scavenging capacity of the CeSACs.

The ·OH scavenging activity of CeSACs was assessed using a microplate reader by evaluating the effective elimination of ·OH generated through the Fenton reaction. A mixture of $FeSO_4$ (1 mmol/L) and H_2O_2 (2 mmol/L) in sodium acetate buffer was prepared, to which different doses of CeSAs (0, 5, 10, and 20 μg/mL) were added. After a reaction period of 5 min, TMB (5 mmol/L) was introduced, and the absorbance of the solution at 650 nm was measured. The ability of CeSACs to scavenge ·OH produced by the Fenton reaction was further corroborated by ESR spectroscopy using the above method.

Ammonium molybdate (AM) was employed for quantification through colorimetric development upon reaction with H_2O_2. H_2O_2 was exposed to varying concentrations of CeSACs (0, 5, 10, and 20 μg/mL) for a duration of 10 min, following which AM was introduced into the system. The absorbance was subsequently measured at a wavelength of 405 nm. Concurrently, the oxygen content within the solution was determined using a dissolved oxygen meter.

The *in vitro* ROS-scavenging activities of LR, CeSACs, LR + CeSACs, and LR@CeSACs were evaluated in equal concentrations by using the above method.

2.10. In vitro ROS-scavenging activities of LR@CeSACs

To investigate the protective effects against H_2O_2-induced oxidative stress, LR, CeSACs, LR + CeSACs, and LR@CeSACs, each at a concentration of 2.5 μg/mL, were cultured with HT29, RAW264.7, and Caco2 cells for 24 h, both in the absence and presence of H_2O_2 (200 μmol/L). Cell viability was assessed using the MTT assay, and phenotypic changes in RAW264.7 cells were analyzed *via* flow cytometry. For confocal imaging and additional flow cytometry assays, HT29, RAW264.7, and Caco2 cells were cultured with the aforementioned materials in the absence or presence of H_2O_2 (400 μmol/L). After a 2-h incubation period, 20 μmol/L dichlorofluorescein diacetate (DCFH-DA) was introduced to assess intracellular ROS generation. Following three washes with PBS, the cells were qualitatively examined using confocal microscopy, and the ROS levels were quantitatively analyzed *via* flow cytometry.

2.11. Catalytic activity and bacterial viability of LR@CeSACs in the GIT

Equal amounts of LR (1×10^7 CFU) and LR@CeSACs (containing 10^7 CFU LR and 50 μg CeSACs) were incubated in 1 mL of medium supplemented with either simulated gastric fluid (SGF) containing pepsin (pH 1.2), simulated intestinal fluid (SIF) containing trypsin (pH 6.8), or simulated colonic fluid (SICF) containing 200 μmol/L H_2O_2 (pH 7.8). The incubation was conducted at 37 °C with gentle shaking to assess their stability within the gastrointestinal environment. At predetermined time points, both the catalytic activity and bacterial viability of LR@CeSACs were evaluated.

For the evaluation of catalytic activities, the samples were subjected to centrifugation, washing, and subsequent redispersion

in PBS to achieve a concentration of 500 μg/mL for both LR@CeSACs and an equivalent amount of LR. Subsequently, their SOD-like and ·OH-scavenging activities were assessed at a final concentration of 50 μg/mL using a total SOD assay kit with WST-8 and TA probes. Additionally, their catalase (CAT)-like performance was evaluated at a final concentration of 100 μg/mL utilizing a CAT assay kit.

To determine bacterial viability, 100 μL of diluted sample was applied to the blood plate at a time. After 48 h of incubation at 37 °C, colonies were counted.

2.12. *Stability of LR@CeSACs in the inflamed colon*

LR@CeSACs was incubated in SICF for varying durations, followed by centrifugation. The resulting precipitates were subsequently washed and subjected to transmission electron microscopy (TEM) analysis to examine the morphological alterations of LR@CeSACs.

2.13. *Ethical approval*

All animal experiments were under the context of the animal protocols approved by the Institutional Animal Care and Use Committee guidelines in Shanghai Tenth Peoples' Hospital (protocol number: SHDSYY-2023-6461). All mice were kept in accordance with the policies on animal research of the National Ministry of Health. All mice used for animal experiments are female with a gentle character, and the sex of the mice does not affect the results of the experiments.

2.14. *In vivo targeting and long-term retention in colon of LR@CeSACs*

To ascertain whether LR probiotics facilitate the targeting of biocompatible CeSACs, *in vivo* imaging was conducted. Specifically, 500 μL of either CeSACs-Cy5.5 or LR@CeSACs-Cy5.5 (each containing 500 μg/mL CeSACs) was orally administered to UC mice. Fluorescence intensities within the intestines of each group were subsequently analyzed utilizing a Lumina Series III *in vivo* imaging system, equipped with a Cy5.5 filter channel and an exposure time of 1 s. For evaluation of retention in colon of LR@CeSACs, UC mice were orally administered 500 μL of either naked LR (1×10^8 CFU/mL) or decorated LR@CeSACs (each containing 500 μg/mL CeSACs and 10^8 CFU/mL LR). After 3 days, the mice subjected to different treatments were euthanized, and their colons were excised for FISH staining and qPCR analysis.

2.15. *In vivo biocompatibility of LR@CeSACs*

LR@CeSACs were administered *via* tail vein injection to female C57BL/6 mice (aged 4−6 weeks, weighing 20−25 g) at doses of 0, 10, and 20 mg/kg. The body weights of the mice were measured and documented on a daily basis. Fourteen days post-injection, blood samples were collected from the mice for serum biochemical tests and blood analysis. The serum biochemical tests assessed two routine indicators of renal function, creatinine (Cre) and blood urea nitrogen (BUN), as well as two routine indicators of hepatic function, alanine aminotransferase (ALT) and aspartate aminotransferase (AST). Additionally, the principal organs (heart, liver, spleen, lungs, and kidneys) of the mice euthanized on Day 14 were collected and subjected to Hematoxylin and Eosin (H&E) staining.

2.16. *Therapeutic efficacy of LR@CeSACs in DSS-induced UC of mice*

Six-week-old female C57BL/6 mice were housed in groups of five per cage and allowed a one-week acclimatization period prior to inclusion in the study. To induce the UC model, mice were administered 3% dextran sulfate sodium (DSS) in their drinking water for four days, followed by a switch to normal water. Control mice were provided with normal water throughout the study. Subsequently, different ratios of LR@CeSACs (LR@CeSACs 25, LR@CeSACs 50, LR@CeSACs 100); 1.25 mg/kg CeSACs, LR, and LR@CeSACs mixture (equivalent dose of LR and CeSACs of LR@CeSACs 50) were administered orally to the mice on predetermined days. Body weight changes were monitored daily over a nine-day experimental period. Fecal samples were collected on a specified day for microbiome analysis. On the final day of the experiment, the mice were euthanized, and the entire colon was excised. The length of the colon was measured, and it was gently washed with physiological saline. Subsequently, two segments of the colon were allocated for histological assessment and immunohistochemical (IHC) staining. The remaining colon tissue samples were utilized for enzyme-linked immunosorbent assay (ELISA) analysis and ROS evaluation. As for the examination of the preventive effect of LR@CeSAC, it was simply a matter of switching the chronological order of feeding the DSS and the various materials as described above. To evaluate the mitigating effect of LR@CeSACs on IBD-induced intestinal fibrosis, the mouse model of intestinal fibrosis by given mice drinking water containing 1% (*w*/*w*) DSS for 8 consecutive weeks. Subsequently, these mice were given different formulations (CeSACs, LR, and LR@CeSACs) orally every week to evaluate their therapeutic effects against intestinal fibrosis.

2.17. *Therapeutic efficacy of LR@CeSACs in TNBS-induced CD of mice*

Female C57BL/6 mice underwent a seven-day acclimatization period before being randomly assigned to various experimental groups, with each group consisting of five mice. Mice subjected to TNBS induction were initially presensitized with 1% (*w*/*w*) TNBS and maintained for seven days. On the eighth day, these mice received an enema with 2% (*w*/*w*) TNBS. Subsequently, treatments involving CeSACs, LR, and LR@CeSACs were administered according to the protocol previously described for the DSS model.

2.18. *Statistics and reproducibility*

For all experiments, the investigators were blinded to group allocation during data collection and/or analysis. For independent experiments with a sample size $n \geq 3$, data are expressed as mean ± standard deviation (SD). Multiple comparisons were conducted using one-way ANOVA, while differences between two groups were analyzed using two-way ANOVA. Statistical analyses were performed and displayed using Graphpad Prism 9.5. *P* values less than 0.05 were considered statistically significant. $^*P < 0.05$, $^{**}P < 0.01$, $^{***}P < 0.001$, $^{****}P < 0.0001$, and ns for non-significant.

3. Results and discussion

3.1. Fabrication and characterization of LR@CeSACs

CeSACs were initially synthesized through the pyrolysis of a Ce-doped metal−organic framework (Fig. 1A). In detail, the Ce-doped zeolitic imidazolate framework (Ce-ZIF) underwent pyrolysis at 950 °C for 1 h. Subsequently, the resulting pyrolysate was subjected to leaching with sulfuric acid to yield CeSACs. To enhance their stability and dispersion, the CeSACs were further functionalized with Silane-PEG-NH_2. The synthesized CeZIF and CeSACs displayed a rhombic dodecahedral morphology with average dimensions of 153 and 126 nm, respectively (Fig. 2A and B, Supporting Information Fig. S1). The Ce element was present as an atomically dispersed species rather than in nanoparticulate form (Fig. 2C−E). Furthermore, XPS and Raman spectroscopy analyses indicated a significant increase in pyridinic N and I_D/I_G (D: disorder; G: graphite) values for CeSACs compared to metal-free carbon nanoparticles (CNPs). The findings indicated that Ce atoms were probably coordinated with pyridinic nitrogen and supported by graphitic carbon (Fig. 2F−H). X-ray absorption fine structure (XAFS) analysis further elucidated the coordination environment. The absorption edge of CeSACs, positioned between those of $CeCl_3$ and CeO_2 (Fig. 2I and J), indicated that the chemical valence of the Ce atom lies between +3 and + 4, which facilitated the cycling of the antioxidant reaction. The peak at 1.8 Å, attributed to Ce−N/O coordination instead of Ce−Ce coordination at 3.6 Å, confirmed the atomic dispersion of Ce within the CeSACs (Fig. 2K and Supporting Information Fig. S2). Wavelet transform analysis of the Ce L-edge EXAFS oscillations revealed the presence of Ce−N structures, with no Ce−Ce bonds detected in the CeSACs (Fig. 2L). EXAFS fitting data quantitatively confirmed that atomic Ce sites are six-coordinated by N/O species (Fig. 2M and Supporting Information Table S1). The Ce atom loading was measured to be 1.83% (*w*/*w*) using inductively coupled plasma mass spectrometry.

LR, a commercially recognized probiotic for modulating intestinal flora, was chosen as the model bacterium in this study. Due to the presence of various amino acid residues, such as carboxyl groups, on the bacterial surface, the PEGylated CeSACs were anchored onto the surface of LR *via* amino acid reactions (Fig. 1A). By functionalizing CeSACs with Silane-PEG-NH_2, the initially prepared CeSACs exhibited enhanced colloidal stability (Supporting Information Figs. S3 and S4). The successful modification of CeSACs by PEG was confirmed by fourier transform infrared spectra (Supporting Information Fig. S5). The LR@CeSACs probiotic system was successfully fabricated by mixing varying proportions of PEG-CeSACs with LR (Fig. 2N and O, Supporting Information Fig. S6). From the bacterial survival experiments, it can be seen that modification with different doses of CeSACs does not cause a significant decrease in the survival of LR (Supporting Information Fig. S7). Among the various candidates, LR@CeSACs was selected for anti-inflammatory evaluation in both *in vitro* and *in vivo* models at a feeding ratio of 1×10^7 CFU LR/50 μg CeSACs. This selection was based on their best bacterial protecting effects (Fig. 3G) and anti-IBD potential (Supporting Information Fig. S8) in a later study. Additionally, LR@CeSACs exhibited strong stability, enabling direct use or storage in an anaerobic tube with the medium (Supporting Information Fig. S9).

3.2. ROS scavenging activities of LR@CeSACs

The ROS scavenging capacity of CeSACs against superoxide anion ($O_2^{\cdot-}$), hydroxyl radical (·OH), and H_2O_2-typical ROS implicated in IBD-was initially examined. As demonstrated in Fig. 3A, CeSACs displayed exceptional concentration-dependent SOD-like activity, effectively catalyzing the disproportionation of $O_2^{\cdot-}$ into H_2O_2 and oxygen (O_2). The generated H_2O_2 can be further eliminated through the catalase-like (CAT-like) properties of CeSACs, as evidenced by the production of O_2 (Fig. 3B). Concurrently, ·OH can be efficiently scavenged *via* the redox cycling between Ce^{3+}/Ce^{4+}, as confirmed by the decreased signal intensity of ·OH in the electron spin resonance (ESR) spectra across different reaction systems (Fig. 3C). Additionally, the superior ROS-scavenging capability of CeSACs was further demonstrated by quantitative scavenging experiments for $O_2^{\cdot-}$, ·OH, and H_2O_2 (Fig. 3D−F). Altogether, CeSACs exhibited a robust reactive oxygen species (ROS) scavenging capacity, attributed to their exceptionally high atomic efficiency and catalytic activities, thereby surpassing other reported antioxidants, particularly CeO_2 (Supporting Information Fig. S10). Consequently, incorporating these antioxidant CeSACs into LR probiotics significantly enhanced the ROS scavenging activity of LR (Fig. 3G−I), ensuring their survival in oxidative stress conditions (Fig. 3J). Additionally, the integration of CeSACs facilitated the maintenance of LR growth in both normal and H_2O_2-mimicking inflammatory environments (Fig. 3K and L).

Following the confirmation of LR@CeSACs's robust ROS-scavenging capability, their *in vitro* antioxidant potential was further evaluated using various cell lines as models. Interestingly, LR demonstrated the ability to promote the proliferation of HT29 and Caco-2 cells (Supporting Information Fig. S11A and S11C), potentially due to its secretion of bioactive factors that hold promise for the repair of intestinal mucosal tissue. Subsequently, under inflammatory conditions, CeSACs, LR + CeSACs, and LR@CeSACs significantly enhanced the viability of HT29 and Caco-2 cells (Fig. S11B and S11D), thereby confirming the cytoprotective properties of the CeSACs component. LR@CeSACs significantly reduced the H_2O_2-induced polarization of RAW264.7 cells to the pro-inflammatory M1 phenotype, indicating a strong immunomodulatory effect (Supporting Information Fig. S12). The findings from fluorescence microscopy and flow cytometry corroborated that the antioxidant and protective mechanisms of LR@CeSACs were attributable to their ROS-scavenging capacity (Fig. 3M and Supporting Information Fig. S13).

3.3. Stability and intestinal targeting capability of LR@CeSACs

Prior to arriving at the inflamed colon, LR@CeSACs are likely to encounter a challenging gastrointestinal (GI) environment following oral administration, which includes factors such as gastric acid, bile salts, and inflammatory conditions. These factors have the potential to destabilize catalysts and deactivate bacteria. Given that the solution may exit the stomach within approximately 20 min, transit through the small intestine for a minimum of 2 h, and ultimately reach the inflamed colon, we assessed the ROS-scavenging capacity and viability of LR and LR@CeSACs after incubation in simulated gastric fluid (SGF) for durations of 10 or 20 min, simulated intestinal fluid (SIF) and simulated inflammatory colon fluid (SICF) for 2 and 4 h. Notably, LR@CeSACs

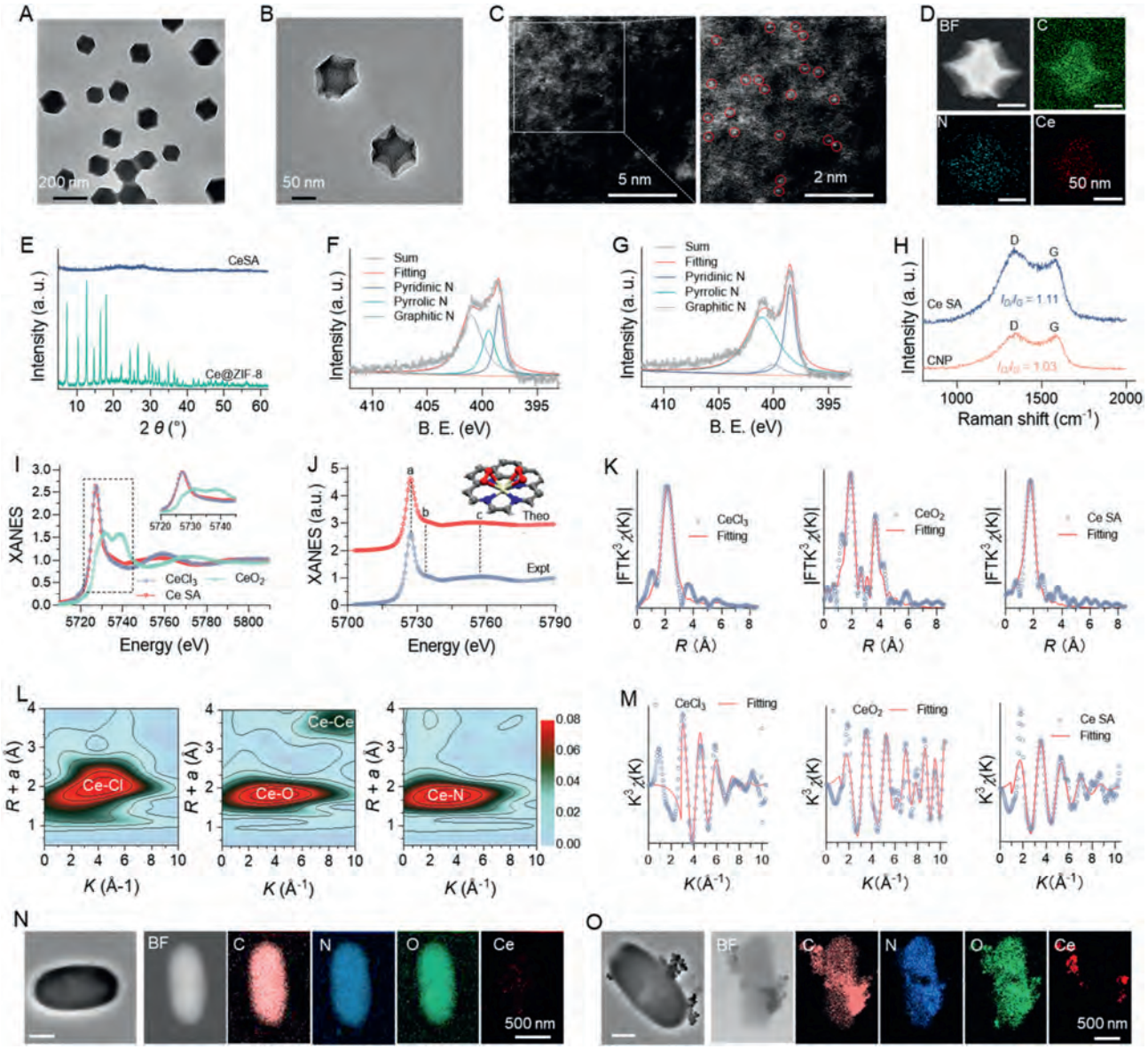

Figure 2 Characterization of different materials. TEM image of (A) Ce-ZIF-8 nanoparticles and (B) CeSACs. (C) AC HAADF-STEM image of CeSACs, with single Ce atoms marked using red circles. (D) HAADF-STEM image and corresponding EDX mappings of CeSACs. (E) XRD patterns of different samples. XPS spectrum of (F) CNP nanoparticles and (G) CeSACs. (H) Raman spectra of different samples. (I) XANES and extracted pre-edge spectra of $CeCl_3$, CeO_2, and CeSACs. (J) Comparison of experimental K-edge XANES spectra of CeSACs with the theoretical spectra derived from CeN_4C_4 moieties within 2D graphene lattice. Key features are highlighted at points a−c. Insert: the teal, blue, grey, and red spheres represent Ce, N, C, and O, respectively. (K) EXAFS fitting in R space of $CeCl_3$, CeO_2, and CeSACs. (L) Wavelet transformation of $CeCl_3$, CeO_2, and CeSACs. (M) EXAFS fitting in K space of $CeCl_3$, CeO_2, and CeSACs. TEM and corresponding elemental mapping images of (N) LR and (O) LR@CeSACs.

maintained stable ROS-scavenging capability across all simulated fluids and time points, significantly outperforming LR, indicating remarkable stability of LR@CeSACs (Fig. 4A−I). Furthermore, the incorporation of CeSACs enhanced the LR survival in SICF without reducing its tolerance in SGF and SIF (Fig. 4J−L). Notably, LR@CeSACs demonstrated significant stability in SICF, indicating its potential for prolonged anti-inflammatory and microbiota-modulating effects in an inflamed colon (Supporting Information Fig. S14).

Next, we evaluated the enhanced intestinal targeting ability of LR@CeSACs using *in vivo* imaging system. Both LR@CeSACs and CeSACs were pre-labeled with Cy5.5 for *in vivo* and *ex vivo* imaging. Upon the oral administration of equivalent quantities of CeSACs and LR@CeSACs, a stronger Cy5.5 fluorescence signal over time was detected in LR@CeSACs-treated colitis mice (Fig. 4M), indicating that LR facilitates the accumulation of CeSACs within the dextran sulfate sodium (DSS)-induced inflamed intestine. Furthermore, the delivery capability of LR for CeSACs was confirmed by imaging analyses of *ex vivo* colonic tissues (Fig. 4N). Moreover, the enhanced targeting capability notably increased the survival of LR in the inflamed colon (Supporting Information Fig. S15). For effective restoration

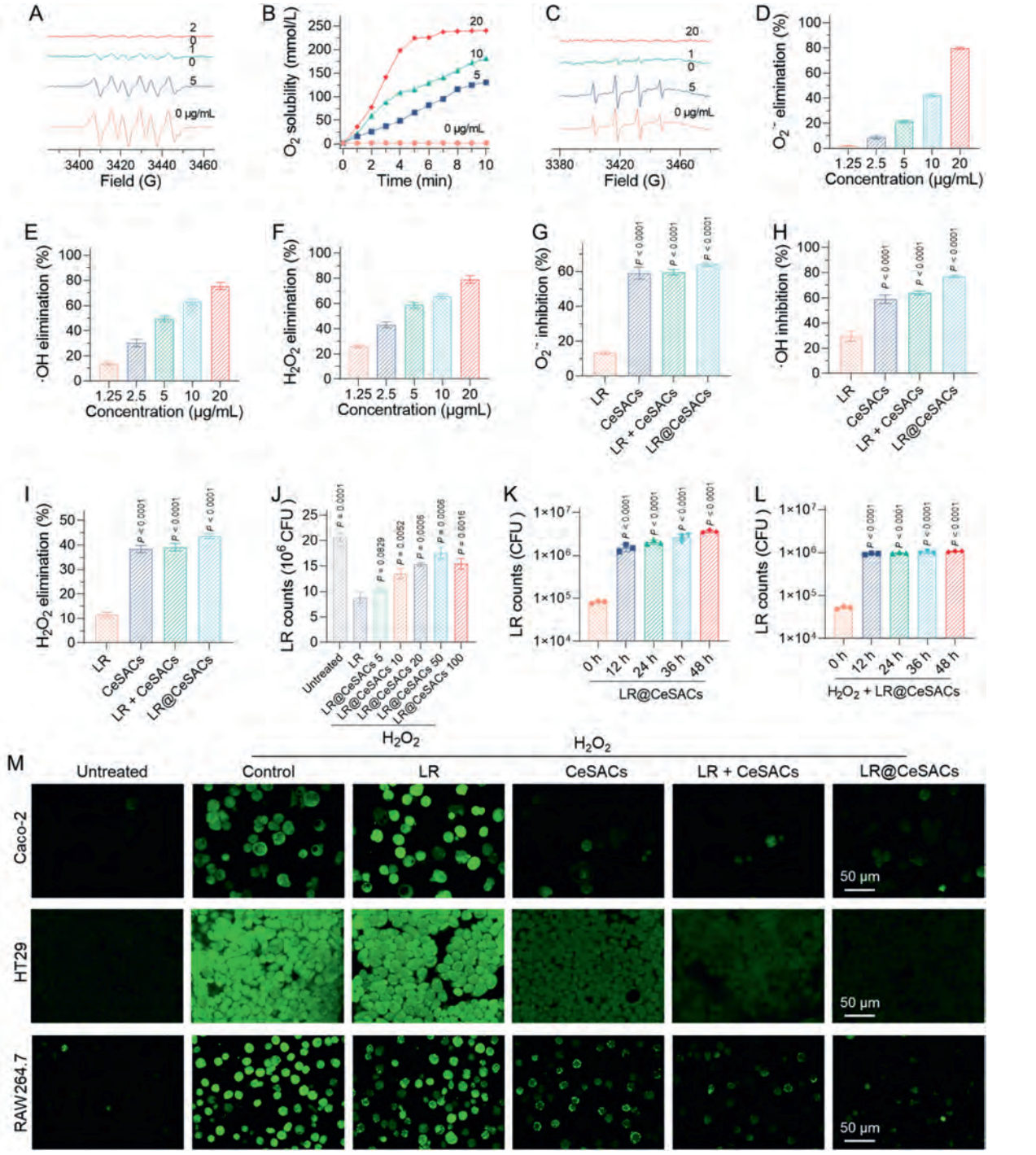

Figure 3 ROS-scavenging activities of LR@CeSACs. (A) ESR spectra of $O_2^{\cdot-}$ after reaction with different doses of CeSACs. (B) Oxygen generation capacity of CeSACs detected by oxygen probe. (C) ESR spectra of ·OH after reaction with different doses of CeSACs. (D) The $O_2^{\cdot-}$ scavenging ability of CeSACs was evaluated using an $O_2^{\cdot-}$-specific total SOD assay kit with WST-8. (E) The efficiency of CeSACs to eliminate ·OH in the Fenton reaction system. (F) H_2O_2-scavenging ability of CeSACs measured by H_2O_2-specific total CAT assay kit. Comparison of (G) $O_2^{\cdot-}$-scavenging ability, (H) ·OH-scavenging ability, and (I) H_2O_2-scavenging ability of different treatments. (J) Survival of LR under the protection of different ratios of CeSACs in 200 μmol/L H_2O_2 for 8 h. Proliferation of LR in LR@CeSACs without (K) or with (L) 200 μmol/L H_2O_2 for different periods of time. (M) Confocal fluorescent images of ROS levels in different cells with different treatments. Cells were stained with ROS probe DCFH-DA (green fluorescence) and DAPI (blue fluorescence). The above experiments were repeated three times. Statistical significance was calculated *via* two independent samples unpaired Student's *t*-test. Data are expressed as mean ± SD. $^*P < 0.05$, $^{**}P < 0.01$, $^{***}P < 0.001$, $^{****}P < 0.0001$.

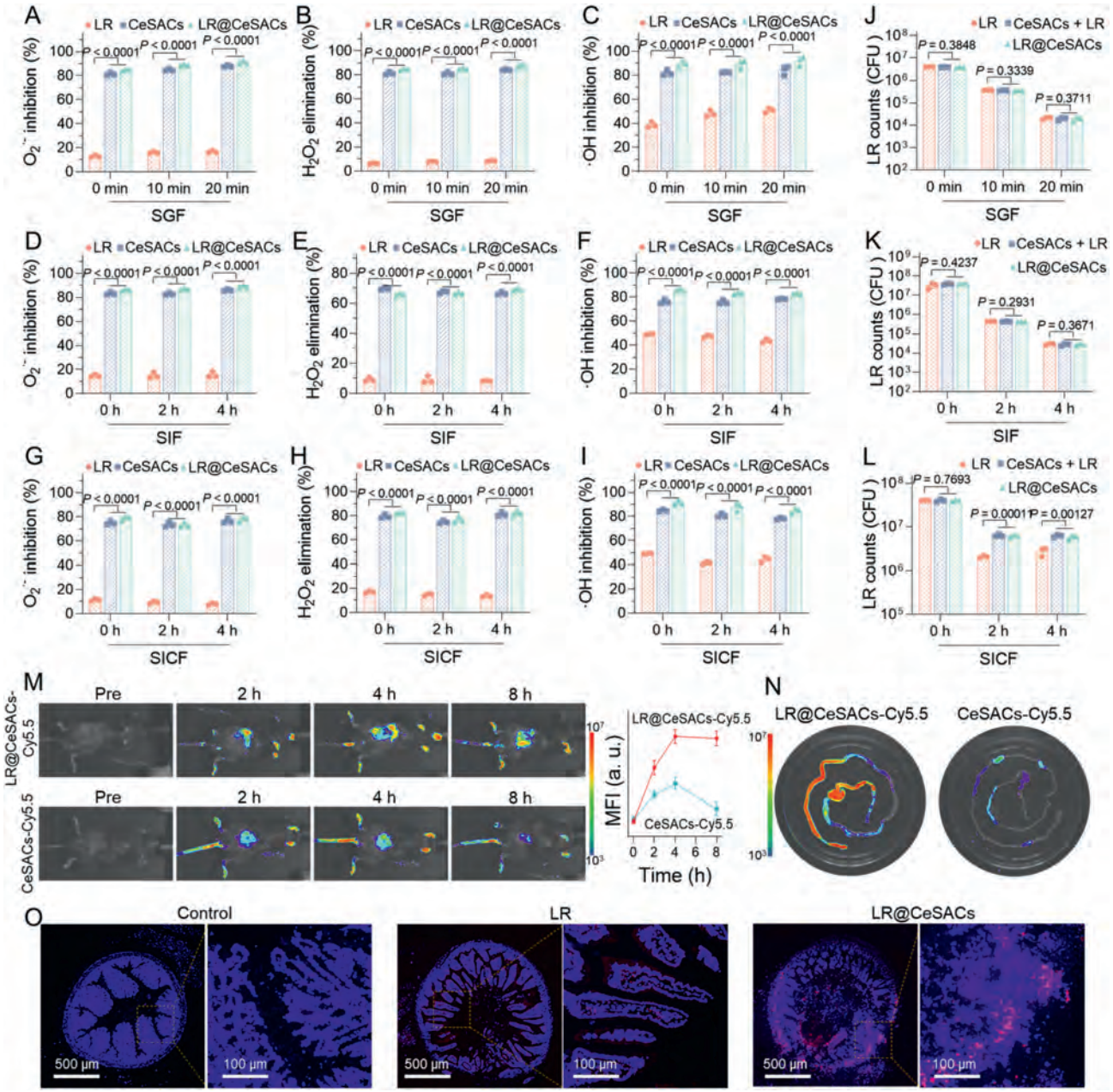

Figure 4 Stability, targeting, and retention of LR@CeSACs in the inflamed colon. Various ROS-scavenging abilities of different materials in simulated (A−C) GI environments of SGF, (D−F) SIF, and (G−I) SICF ($n = 3$). Corresponding viability of LR in (J) SGF, (K) SIF, and (L) SICF. (M) *In vivo* imaging of mice ($n = 3$) conducted at 2, 4, and 8 h following oral administration of CeSACs and LR@CeSACs. (N) The *ex vivo* fluorescence imaging of the colon at 8 h after oral administration of CeSACs and LR@CeSACs. (O) Representative fluorescence *in situ* hybridization (FISH) assay images showing LR levels in the colon of IBD mice ($n = 3$) three days post-administration of LR and LR@CeSACs. Blue fluorescence indicates colon cells, while red fluorescence signifies LR. Statistical significance was calculated *via* two independent samples unpaired Student's *t*-test. Data are expressed as mean ± SD. $^{*}P < 0.05$, $^{**}P < 0.01$, $^{***}P < 0.001$, $^{****}P < 0.0001$.

of intestinal barrier integrity and gut microbiota functionality, LR@CeSACs must persist and replicate within the intestinal tract for an extended period. The FISH analysis of colon tissue sections (Fig. 4O and Supporting Information Fig. S16) revealed the presence of LR within the colon tissues of (UC) mice treated with LR, CeSACs + LR, and LR@CeSACs, predominantly localized in the mucus layer. Notably, the LR@CeSACs group exhibited a significantly higher fluorescence intensity compared to the LR group, likely due to the protective effect of LR@CeSACs on LR in the inflamed colon. However, this result was also supported by the results of quantitative polymerase chain reaction (qPCR) analysis, in which the number of BL in the LR@CeSACs group was significantly higher than that in the BL group (Supporting Information Fig. S17).

3.4. *In vivo biosafety of LR@CeSACs*

A systematic *in vivo* toxicology evaluation of LR@CeSACs was conducted to ensure their safe bioapplications. Healthy mice received daily oral doses of LR@CeSACs (0, 5×10^7, and

2.5×10^8 CFU/kg) for a month. Subsequently, weight changes, a series of biochemical and hematological parameters, and hemoglobin and eosin (H&E) staining of major organs of mice in different groups were examined (Supporting Information Fig. S18). No significant difference was observed between the two experimental groups and the control group, showing negligible toxicity of LR@CeSACs.

3.5. Therapeutic efficacy of LR@CeSACs against IBD

To access the therapeutic efficacy of LR@CeSACs against UC, we established a mouse colitis model by administering 3% (*w*/*w*) DSS in drinking water for four consecutive days, which is directly toxic to the intestinal basal cryptepithelial cells and compromise mucosal barrier integrity[32,33]. Subsequently, these UC mice were orally administered varying doses of the LR@CeSACs formulation over four days to identify the most effective therapeutic candidates. It was evident that a dosage of 2.5 mg/kg of LR@CeSACs at a feeding ratio of 10^7 CFU LR/50 μg CeSACs exhibited the most pronounced therapeutic effect on colitis and was therefore selected for further investigation (Supporting Information Figs. S8 and S19). Subsequently, the efficacy of selected LR@CeSACs was assessed in comparison to other treatments following the protocol displayed in Fig. 5A. Oral administration of LR@CeSACs significantly mitigated weight loss, reduced the disease activity index (DAI), prevented colon shortening, and alleviated fecal abnormalities in mice with colitis (Fig. 5B−E). In contrast, the anti-IBD effects of the other preparations were comparatively diminished. In addition, H&E and IHC analysis revealed that LR@CeSACs treatment safeguarded the colon epithelium from pathological damage and suppressed IL-6 and TNF-α expression. Meanwhile, LR@CeSACs significantly decreased reactive oxygen species (ROS) levels and pro-inflammatory factors (IL-6, IFN-γ, MPO), while increasing anti-inflammatory factor IL-10, as shown by ROS staining and enzyme-linked immunosorbent assay (Fig. 5F and G, and Fig. 5H−K). Finally, LR@CeSACs treatment significantly prolonged the survival cycle of UC mice without causing obvious damage to major organs (Fig. 5L, and Supporting Information Fig. S20). We evaluated the therapeutic efficacy of LR@CeSACs against CD, another major form of IBD in humans.

To establish a CD mouse model, 2,4,6-trinitrobenzene sulfonic acid (TNBS) was administered intrarectally. TNBS is known to induce a T-cell-mediated response against hapten-modified autologous proteins and luminal antigens (Supporting Information Fig. S21A). On Day 9, significant body-weight loss and bleeding were observed, indicating the successful induction of CD (Fig. S21B). Subsequently, these CD mice were orally administered various materials over four days. Comparative analyses of changes in body weight, DAI, and colon lengths suggested that LR@CeSACs exhibited potentially greater therapeutic efficacy compared to other formulations (Fig. S21C and S21D). Taken together, LR@CeSACs exhibited excellent efficacy in the treatment of IBD owing to the synergistic effect of CeSACs and LR in the combination.

3.6. Modulation of gut microbiome by LR@CeSACs

To test if LR@CeSACs could mitigate gut microbiota dysbiosis, we employed 16S ribosomal RNA gene sequencing in the V4 regions to analyze the temporal dynamics of the gut microbiota during treatment. DSS administration significantly and swiftly altered the mouse microbiota, evidenced by reductions in Chao1 and other biodiversity indices (Fig. 6A−D), which was also demonstrated by alterations in the composition of the microbiota of isolated clusters in the non-metric multidimensional scalar plot (Supporting Information Fig. S22). Further family-level and phylum-level analysis (Fig. 6E and F) demonstrated that DSS significantly decreased the relative abundance of *Bacteroides* and Lactobacillaceae while increasing the relative abundance of Proteobacteria and Enterobacteriaceae typically associated with dysbiosis in IBD patients[34]. However, bacterial diversity and community dysbiosis were significantly improved after antioxidant or bacterial therapy. In particular, LR@CeSACs-mediated treatment significantly enhanced the relative abundance of beneficial flora and reduced the relative abundance of harmful flora in DSS colitis mice. The long-term exposure to LR@CeSACs did not result in an overgrowth of beneficial taxa or rebound proliferation of pathogens (Supporting Information Fig. S23).

The bacterial composition of treated colitis mice was further revealed in detail at the portal and section level (Fig. 6G−N). LR@CeSACs significantly increased the relative abundance of Firmicutes, including the Lactobacillaceae, Muribaculaceae, and Bifidobacteriaceae families, promoting a beneficial shift in IBD health[35]. The Muribaculaceae, strongly correlated with propionate, can inhibit $CD8^+$ T cell activation, thus suppressing immunogenic inflammation. Bifidobacteriaceae is linked to butyric acid production, which promotes inflammation regression and supports the growth of microorganisms and host epithelial cells[36]. LR@CeSACs reduced the relative abundance of potentially pathogenic Proteobacteria, including the Enterobacteriaceae, Erysipelotrichaceae, and Escherichia-Shigella families, all of which are associated with inflamed gut environments and may exacerbate the inflammatory response in IBD[37]. To further interpret the observed differences in microbiome composition, a linear discriminant analysis (LDA) effect size (LEfSe) analysis was conducted (Fig. 6O and Supporting Information Fig. S24). Consistent with prior analysis, LR@CeSACs treatment led to a notable increase in Firmicutes abundance and a significant reduction in IBD-associated Proteobacteria.

3.7. Alleviation of intestinal fibrosis by LR@CeSACs

To evaluate the mitigating effect of LR@CeSACs on IBD-induced intestinal fibrosis, we first established a mouse model of intestinal fibrosis by giving mice drinking water containing 1% (*w*/*w*) DSS for 8 consecutive weeks (Fig. 7A). Subsequently, these mice were given different formulations orally every week to evaluate their therapeutic effects against intestinal fibrosis. As expected, LR@CeSACs significantly mitigated weight loss and reduced the DAI (Fig. 7B and C), as well as infiltration of inflammatory cells (Fig. 7E), indicating the favorable relief of inflammation. In particular, LR@CeSACs remarkably halted the colon narrowing which is a typical mark of intestinal fibrosis (Fig. 7D and Supporting Information Fig. S25). In contrast, the anti-colon narrowing effects of the other treatments were comparatively diminished. Furthermore, IHC analysis (Fig. 7F and G) showed that LR@CeSACs more effectively suppressed the expression of fibrosis markers, such as α-SMA and Tnc, compared to other treatments[38]. Picrosirius red/fast yellow staining was used to quantify collagen content in the colon. Collagen deposition, indicative of potential intestinal fibrosis, was observed in DSS-treated mice but not in those treated with LR@CeSACs (Fig. 7H). Additionally, a qPCR array of fibrosis-related genes

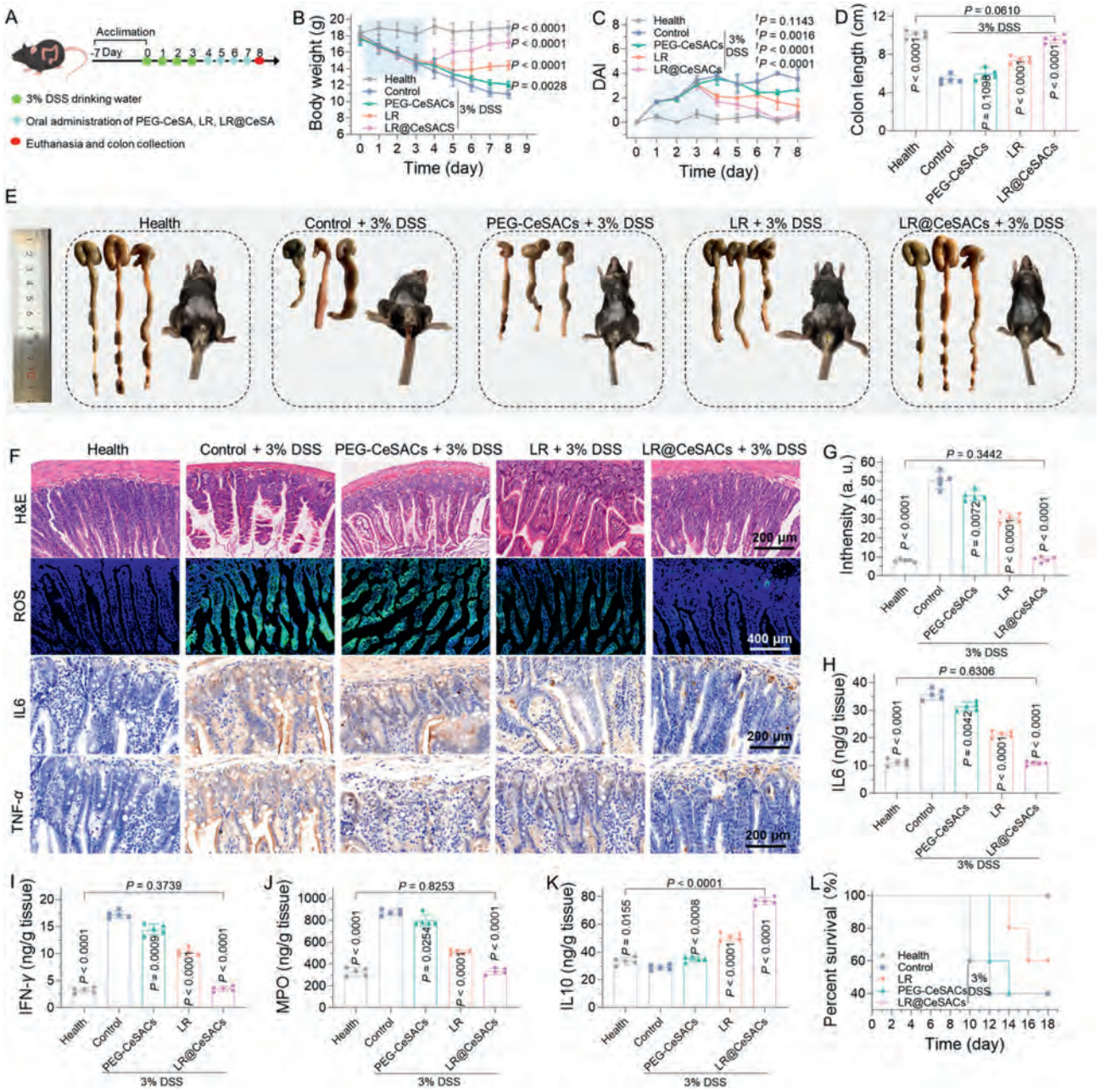

Figure 5 LR@CeSACs alleviate DSS-induced UC. (A) C57BL/6 mice were provided with water or 3% DSS-containing water for 4 days. On Days 4, 5, 6, and 7, mice ($n = 5$) were orally administered with PBS or PBS containing CeSACs (2 mg/kg), LR (3×10^8 CFU/kg), or LR@CeSACs (LR, 3×10^8 CFU/kg; CeSACs, 2 mg/kg). (B) Daily body-weight changes of mice in different groups ($n = 5$) for 9 days. (C) Changes in DAI of mice in different groups ($n = 5$), which is the average of the stool consistency index (0−3), fecal bleeding index (0−3), and weight loss index (0−4). (D) Colon lengths of mice in different groups ($n = 5$) on Day 8. (E) Digital photographs of the anal and isolated colon of mice on Day 8 after different treatments. (F) H&E-staining and IHC analysis of colonic sections of mice on Day 8 after different treatments. (G) Relative ROS levels in colons of mice on Day 8 after the indicated treatments. (H−K) The inflammatory cytokines levels in colons of mice ($n = 5$) on Day 8 after different treatments. (L) Survival rate of mice ($n = 10$) in 18 days after the indicated treatments. Statistical significance was calculated *via* two independent samples unpaired Student's *t*-test. Data are expressed as mean ± SD. $^*P < 0.05$, $^{**}P < 0.01$, $^{***}P < 0.001$, $^{****}P < 0.0001$.

was conducted to evaluate the antifibrosis effects of LR@CeSACs on IBD mice in gene levels. A series of genes related to inflammatory and fibrotic processes[39] were upregulated after the administration of DSS compared to the levels observed in the control group, while these genes expression was inhibited by LR@CeSACs (Fig. 7I). Overall, LR@CeSACs are capable of effectively managing the IBD complications of intestinal fibrosis by suppressing inflammation and restoring the balance of intestinal flora.

3.8. *Prophylactic efficacy of LR@CeSACs against IBD*

Motivated by the promising therapeutic effects of LR@CeSACs on IBD, we explored their prophylactic potential in preventing

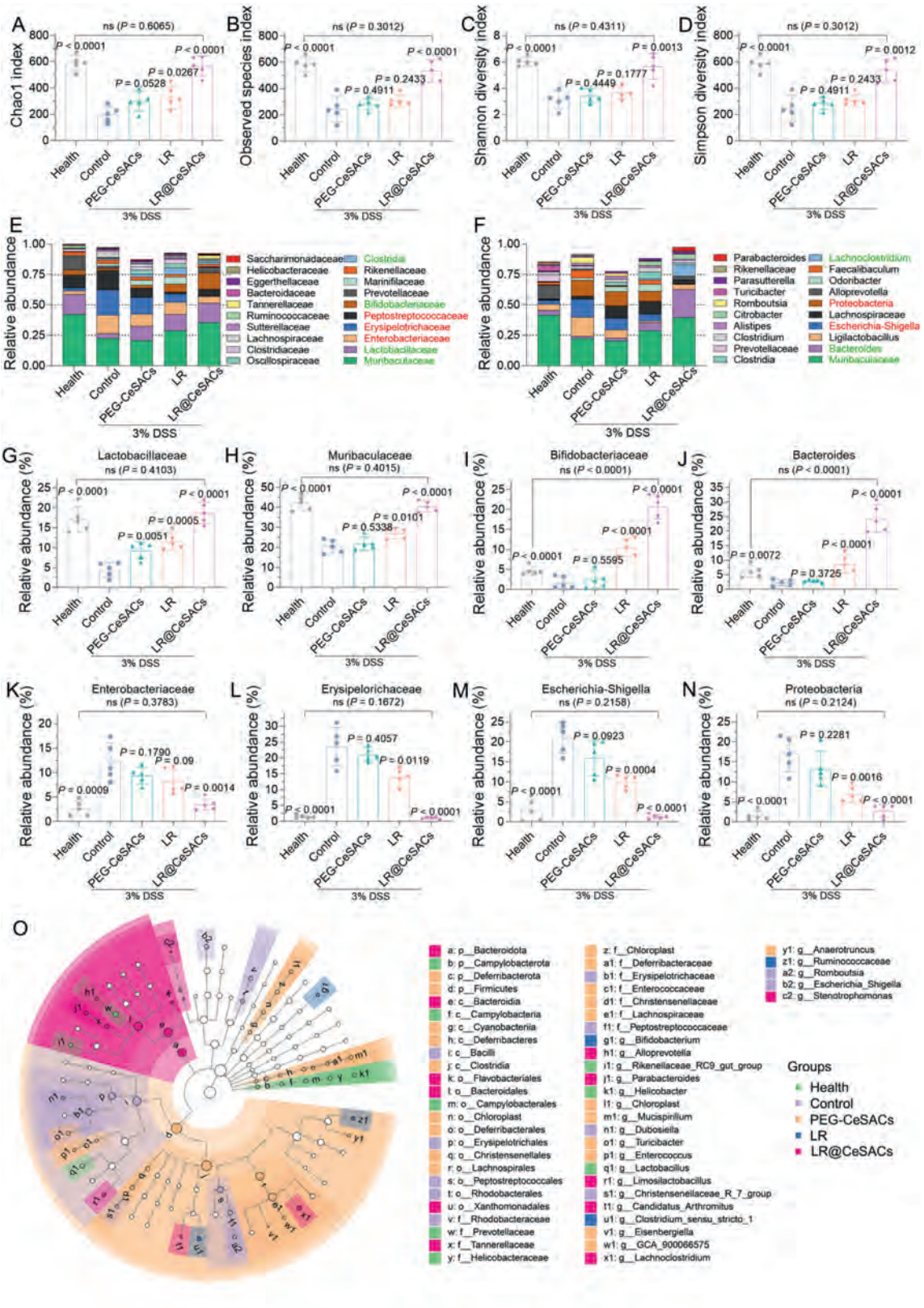

Figure 6 LR@CeSACs modulating the gut microbiota of UC. (A−D) The diversity of faecal microbiome illustrated by different indexes after different treatments ($n = 3$). Relative abundance of gut microbiome illustrated at the (E) family-level and (F) phylum-level taxonomy after different treatments. (G−N) Relative abundance of select taxa at the phylum-level taxonomy and family level after different treatments. (O) Cladogram based on LEfSe analysis showing the community composition of the gut microbiota in mice with different treatments. Statistical significance was calculated *via* two independent samples unpaired Student's *t*-test. Data are expressed as mean ± SD. $^{*}P < 0.05$, $^{**}P < 0.01$, $^{***}P < 0.001$, $^{****}P < 0.0001$.

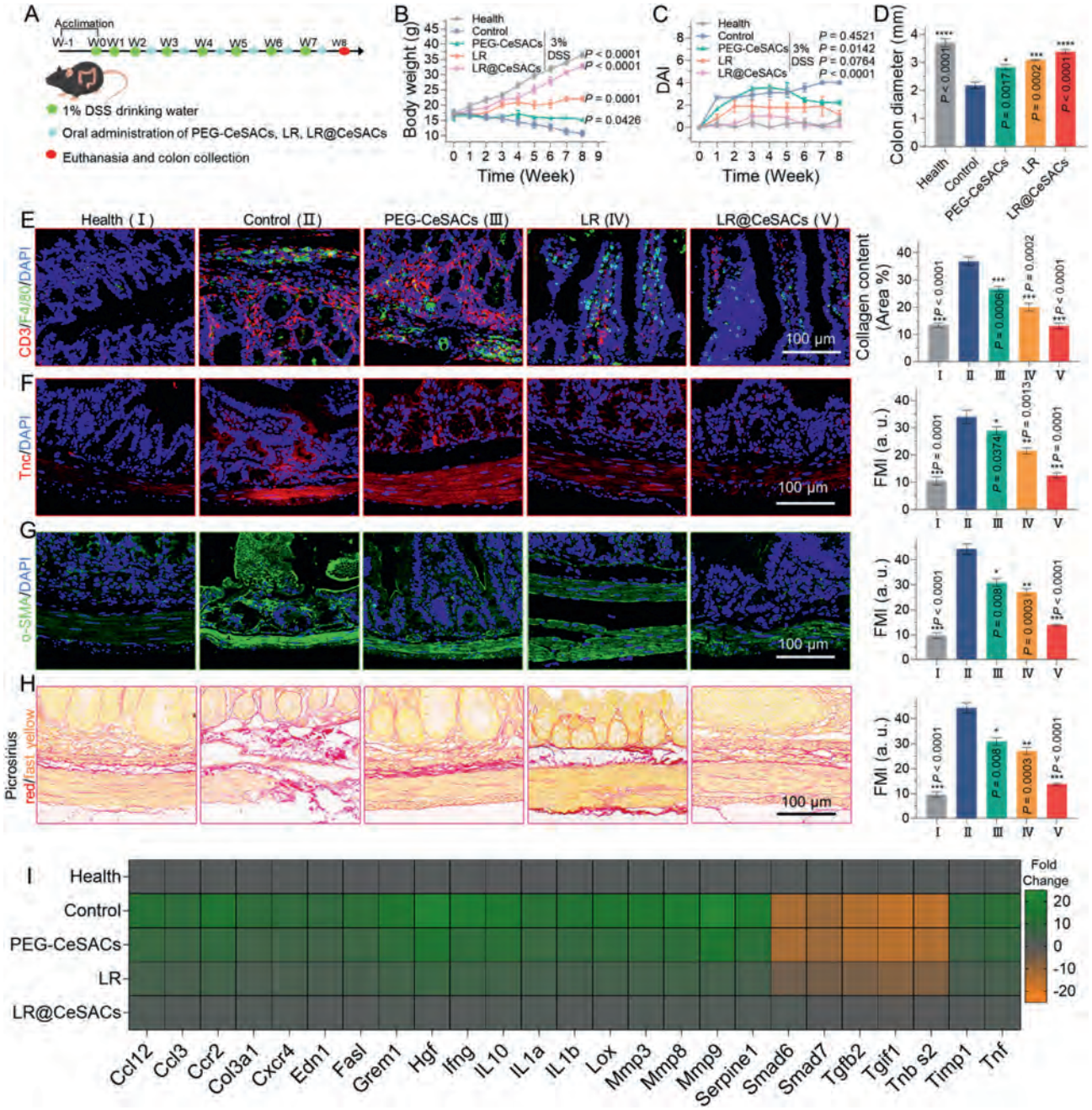

Figure 7 LR@CeSACs alleviate DSS-induced intestinal fibrosis. (A) C57BL/6 mice were provided with 1% DSS-containing for 7 weeks. On first day of Weeks 2−7, mice ($n = 5$) were orally administered with PBS or CeSACs (2 mg/kg), LR (3×10^8 CFU/kg), or LR@CeSACs (LR, 3×10^8 CFU/kg; CeSACs, 2 mg/kg) containing PBS. (B) Daily body-weight changes of mice ($n = 5$) in different groups for 8 days. (C) Changes in DAI of mice in different groups. (D) Colon and spleen lengths of mice in different groups ($n = 5$) on Day 8. (E) Immunofluorescence labeling of CD3/F4/80 positive immune cells (F) TNC (red fluorescence), and (G) α-SMA (green fluorescence) in colon sections of different groups ($n = 3$) and their quantifications. (H) Representative images of Picrosirius Red/Fast yellow staining and corresponding quantitative analysis of the collagen content among the different groups. (I) RNA expression of genes involved in fibrosis in colon tissues of different groups ($n = 3$) determined by PCR assay. Heat maps showed the significantly upregulated (green) or downregulated (yellow) genes in different groups. Statistical significance was calculated *via* two independent samples unpaired Student's *t*-test. Data are expressed as mean ± SD. $^*P < 0.05$, $^{**}P < 0.01$, $^{***}P < 0.001$, $^{****}P < 0.0001$.

colitis in mice. Mice were orally administered various LR and CeSACs-based formulations for 5 days, followed by 7 days of drinking water containing 3% DSS to induce colitis (Fig. 8A). Notably, the mice treated with LR@CeSACs showed substantially less weight loss (Fig. 8B), reduced DAI (Fig. 8C), prevented colon shortening (Fig. 8E and F), and relieved splenomegaly (Fig. 8G) compared to the other treatment groups. Histopathological analysis of H&E stained colon tissue further confirmed that LR@CeSACs significantly prevented IBD, showing less disruption in the epithelial barrier and crypts in LR@CeSACs-treated

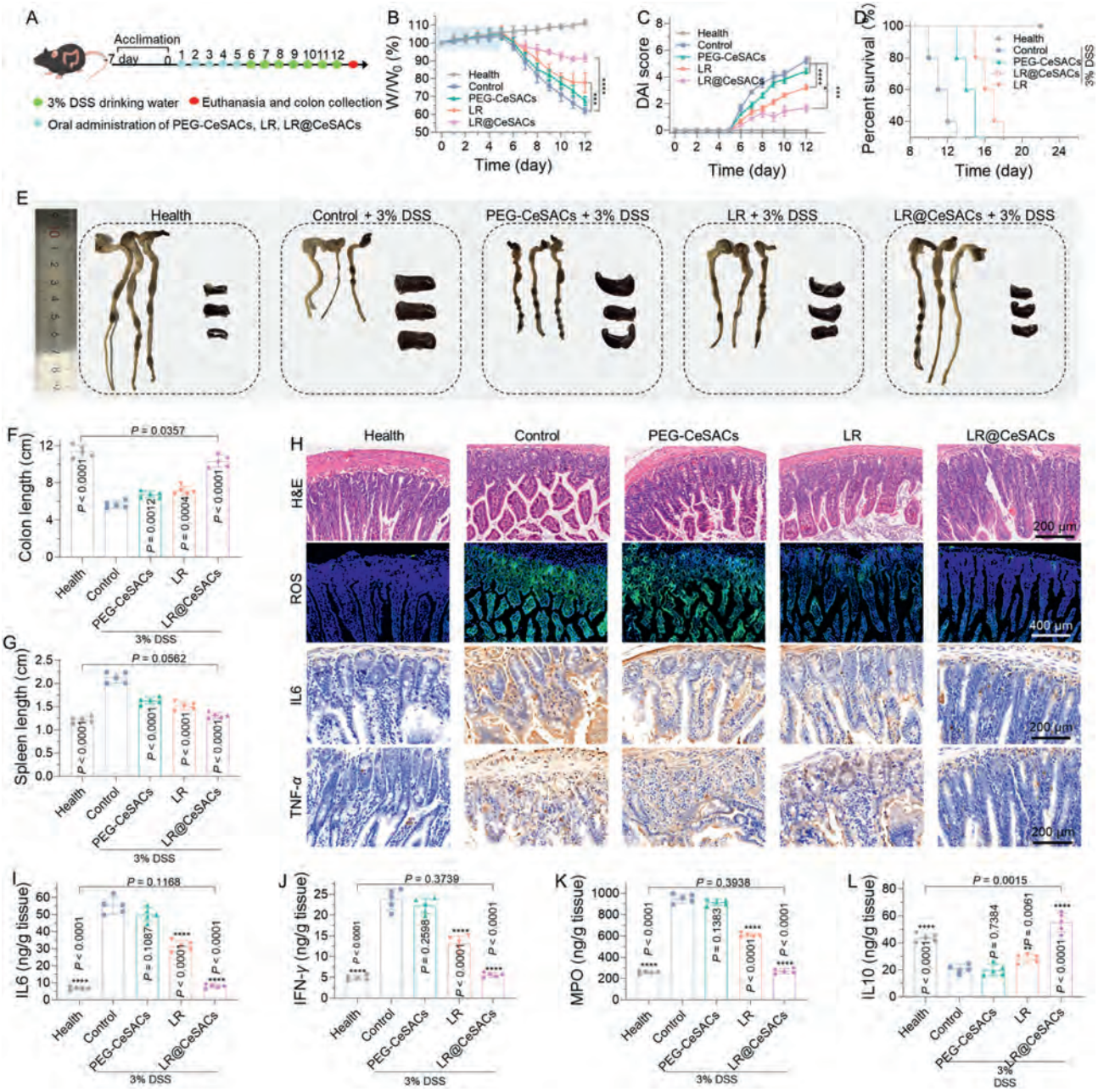

Figure 8 LR@CeSACs prevent DSS-induced UC. (A) C57BL/6 mice ($n = 5$) were provided with water or CeSACs (2 mg/kg), LR (3×10^8 CFU/kg), or LR@CeSACs (LR, 3×10^8 CFU/kg; CeSACs, 2 mg/kg) containing water for 5 days. On Days 6−12, mice were orally administered with 3% DSS-containing water. (B) Daily body-weight changes of mice in different groups for 12 days. (C) Changes in DAI of mice ($n = 5$) in different groups. (D) The survival rate of mice ($n = 10$) in 22 days after the indicated treatments. (E) Digital photographs of isolated colon and spleen of mice ($n = 3$) on Day 12 after different treatments. (F) Colon and (G) spleen lengths of mice in different groups on Day 8. (H) H&E-staining, relative ROS, and IHC analysis of colonic sections of mice on Day 12 after different treatments. (I−L) The inflammatory cytokines levels in colons of mice on Day 12 after different treatments ($n = 5$). Statistical significance was calculated *via* two independent samples unpaired Student's *t*-test. Data are expressed as means ± SD. $^*P < 0.05$, $^{**}P < 0.01$, $^{***}P < 0.001$, $^{****}P < 0.0001$.

mice compared to other treatments. This preventive effect of LR@CeSACs on IBD may be due to that they could reside in the intestinal site for an extended time to effectively reduce ROS levels (Fig. 8H) at the infection site, inhibiting pro-inflammatory cytokine release and up-regulating anti-inflammatory cytokine release when challenged by DSS-induced inflammation (Fig. 8I−L). As a result, mice treated with LR@CeSACs were able to survive beyond the observed 22 days, during which all mice in the other panels already died (Fig. 8D).

4. Conclusions

Concurrently repairing the inflammation-induced barrier dysfunction of the gut mucosa and reshaping the balance of the gut

microbiota is critical for IBD therapy. However, traditional clinical treatments for IBD, such as certain anti-inflammatory medications and probiotics, are ineffective and may cause serious side effects with long-term use, decreasing patients' quality of life and increasing the risk of serious diseases such as colon cancer[11-13]. In this study, a novel antioxidant CeSACs was first developed to mimic the natural antioxidant defense systems to replace clinically used anti-inflammatory drugs and further used to arm LR probiotics to rapidly and effectively reshape the pathological microenvironment of IBD. Compared with clinical drugs, LR@CeSACs formulations not only offered the advantages of sustained cascade catalysis and biosafety to scavenge ROS to reduce inflammation but also enhanced bacterial viability and rapidly remodeled gut barrier function and gut microbiota. Moreover, the retention time of CeSACs catalysts in the inflamed gut was prolonged due to the inherent colonization ability of LR probiotics. Therefore, LR@CeSACs effectively reduced ROS and inflammation, repaired the intestinal barrier, and regulated the microbiota in DSS-induced UC and TNBS-induced CD mice. In addition, LR@CeSACs significantly down-regulated pro-fibrosis-related genes, effectively alleviating IBD-induced intestinal fibrosis, a common complication of IBD, and demonstrated a preventive effect on IBD. It is notable that the mice did not show any adverse effects after repeated treatment with LR@CeSACs during treatment, which further facilitates its clinical translation. In conclusion, the engineered LR probiotic developed in this study advances the use of artificial catalysts and metabolic probiotics in creating an anti-inflammatory oral formulation for the comprehensive treatment of IBD.

Data availability statement

This study utilizes publicly accessible data from the Protein Data Bank (PDB) under accession code: 1DGF (https://doi.org/10.2210/pdb1DGF/pdb). A reporting summary for this article can be found in the Supporting Information.

Acknowledgments

We greatly acknowledge the financial support from National Natural Science Foundation of China (Grant Nos. 82402302, 82022033, and 52402353), Sichuan Science and Technology Program (2024NSFSC1776, China), Chengdu Science and Technology Program (Grant No. 2024-YF0501722-SN, China), and Shanghai Sailing Program (Grant No. 3YF1454500, China). The authors thank Figdraw (www.figdraw.com) for their help in creating the images and EditSprings (https://www.editsprings.cn) for their expert linguistic services.

Author contributions

Yinying Pu, Shaorong Huang, and Shuang Gao contributed equally to this work. Wencheng Wu, Kun Zhang, and Min Zhou conceived and designed the study. Yinying Pu, Shaorong Huang, and Shuang Gao designed and synthesized the materials, performed the structural characterizations and catalytic experiments, and analyzed the data. Wenhao Li and Qiyue Li performed the *in vitro* and *in vivo* study, and analyzed the data. Yangying Duan and Han Lin assisted with the *in vitro* and *in vivo* study. Wencheng Wu, Kun Zhang, Min Zhou, Yinying Pu, Shaorong Huang, and Shuang Gao analyzed the results and wrote the paper. All the authors discussed the results and commented on the manuscript.

Conflicts of interest

The authors declare no conflicts of interest.

Appendix A. Supporting information

Supporting information to this article can be found online at https://doi.org/10.1016/j.apsb.2025.06.022.

References

1. Stournaras E, Qian WD, Pappas A, Hong YY, Shawky R, Raine T, et al. Thiopurine monotherapy is effective in ulcerative colitis but significantly less so in Crohn's disease: long-term outcomes for 11928 patients in the UK inflammatory bowel disease bioresource. *Gut* 2021; **70**:677−86.
2. Scott BM, Gutiérrez-Vázquez C, Sanmarco LM, da Silva Pereira JA, Li Z, Plasencia A, et al. Self-tunable engineered yeast probiotics for the treatment of inflammatory bowel disease. *Nat Med* 2021;**27**:1212−22.
3. Zhao PC, Xia XF, Xu XY, Leung KKC, Rai AZ, Deng YR, et al. Nanoparticle-assembled bioadhesive coacervate coating with prolonged gastrointestinal retention for inflammatory bowel disease therapy. *Nat Commun* 2021;**12**:7162.
4. D'Alessio S, Ungaro F, Noviello D, Lovisa S, Peyrin-Biroulet L, Danese S. Revisiting fibrosis in inflammatory bowel disease: the gut thickens. *Nat Rev Gastroenterol Hepatol* 2022;**19**:169−84.
5. Meng Q, Guo JS, Lv K, Liu Y, Zhang J, Li M, et al. 5*S*-Heudelotinone alleviates experimental colitis by shaping the immune system and enhancing the intestinal barrier in a gut microbiota-dependent manner. *Acta Pharm Sin B* 2024;**14**:2153−76.
6. Citi S. Intestinal barriers protect against disease. *Science* 2018;**359**: 1097−8.
7. Chu H, Khosravi A, Kusumawardhani IP, Kwon AHK, Vasconcelos AC, Cunha LD, et al. Gene−microbiota interactions contribute to the pathogenesis of inflammatory bowel disease. *Science* 2016;**352**:1116−20.
8. Jing WG, Dong SJ, Xu YY, Liu JJ, Ren JW, Liu X, et al. Gut microbiota-derived tryptophan metabolites regulated by Wuji Wan to attenuate colitis through AhR signaling activation. *Acta Pharm Sin B* 2024;**15**:205−23.
9. Wang MY, Huang Q, Liu M, Zhao TJ, Song XP, Chen QH, et al. Precisely inhibiting excessive intestinal epithelial cell apoptosis to efficiently treat inflammatory bowel disease with oral pifithrin-α embedded nanomedicine. *Adv Mater* 2023;**35**:2309370.
10. Plichta DR, Graham DB, Subramanian S, Xavier RJ. Therapeutic opportunities in inflammatory bowel disease: mechanistic dissection of host−microbiome relationships. *Cell* 2019;**178**:1041−56.
11. Lautenschläger C, Schmidt C, Fischer D, Stallmach A. Drug delivery strategies in the therapy of inflammatory bowel disease. *Adv Drug Deliv Rev* 2014;**71**:58−76.
12. Cader MZ, Kaser A. Finding the right target for drug-resistant inflammatory bowel disease. *Nat Med* 2021;**27**:1870−1.
13. Bernstein CN, Fried M, Krabshuis JH, Cohen H, Eliakim R, Fedail S, et al. World gastroenterology organization practice guidelines for the diagnosis and management of IBD in 2010. *Inflamm Bowel Dis* 2010; **16**:112−4.
14. Mishra P, Lee J, Kumar D, Louro RO, Costa N, Pathania D, et al. Engineered nanoenzymes with multifunctional properties for next-generation biological and environmental applications. *Adv Funct Mater* 2022;**32**:2108650.
15. Lu D, Wu Q, Xu XS, Lyu Q, Liu C, Yuan HX, et al. Antioxidative single atomic nanocatalysts facilitate orally administered probiotic inulin gels for acute colitis amelioration. *Nano Today* 2024;**55**:102150.

16. Du YJ, Huo Y, Yang Q, Han ZH, Hou LQ, Cui BX, et al. Ultrasmall iron-gallic acid coordination polymer nanodots with antioxidative neuroprotection for PET/MR imaging-guided ischemia stroke therapy. *Exploration (Beijing)* 2023;**3**:20220041.
17. Yang J, Zhang RF, Zhao HQ, Qi HF, Li JY, Li JF, et al. Bioinspired copper single-atom nanozyme as a superoxide dismutase-like antioxidant for sepsis treatment. *Exploration (Beijing)* 2022;**2**:20210267.
18. Zhao S, Li YX, Liu QY, Li SR, Cheng Y, Cheng CQ, et al. An orally administered CeO_2@Montmorillonite nanozyme targets inflammation for inflammatory bowel disease therapy. *Adv Funct Mater* 2020;**30**:2004692.
19. Cao FF, Jin LL, Gao Y, Ding Y, Wen HY, Qian ZF, et al. Artificial-enzymes-armed *Bifidobacterium longum* probiotics for alleviating intestinal inflammation and microbiota dysbiosis. *Nat Nanotechnol* 2023;**18**:617−27.
20. Liu YF, Cheng Y, Zhang H, Zhou M, Yu YJ, Lin SC. Integrated cascade nanozyme catalyzes *in vivo* ROS scavenging for anti-inflammatory therapy. *Sci Adv* 2020;**6**:eabb2695.
21. Liu TF, Xiao BW, Xiang F, Tan JL, Chen Z, Zhang XR, et al. Ultrasmall copper-based nanoparticles for reactive oxygen species scavenging and alleviation of inflammation related diseases. *Nat Commun* 2020;**11**:2788.
22. Liu J, Shi L, Wang Y, Li MY, Zhou C, Zhang LF, et al. Ruthenium-based metal-organic framework with reactive oxygen and nitrogen species scavenging activities for alleviating inflammation diseases. *Nato Today* 2022;**47**:101627.
23. Pu YY, Duan YY, Li WH, Lin H, Li QY, Yin BY, et al. A cerium single-atom catalyst enables targeted catalytic therapy for acute kidney injury *via* neutrophil hitchhiking. *J Control Release* 2025;**380**:404−16.
24. Xue ZH, Luan D, Zhang H, Lou XW. Single-atom catalysts for photocatalytic energy conversion. *Joule* 2022;**6**:92−133.
25. Chang BS, Zhang LQ, Wu SR, Sun ZY, Cheng Z. Engineering single-atom catalysts toward biomedical applications. *Chem Soc Rev* 2022; **51**:3688−734.
26. Tong ZR, Gao Y, Yang H, Wang WL, Mao ZW. Nanomaterials for cascade promoted catalytic cancer therapy. *View* 2021;**2**:20200133.
27. Jostins L, Ripke S, Weersma RK, Duerr RH, McGovern DP, Hui KY, et al. Host−microbe interactions have shaped the genetic architecture of inflammatory bowel disease. *Nature* 2012;**491**:119−24.
28. Han K, Nam J, Xu J, Sun X, Huang X, Animasahun O, et al. Generation of systemic antitumour immunity *via* the *in situ* modulation of the gut microbiome by an orally administered inulin gel. *Nat Biomed Eng* 2021;**5**:1377−88.
29. Luo M, Hu MM, Feng X, Wu XL, Dong DG, Wang WC. Preventive effect of *Lactobacillus reuteri* on melanoma. *Biomed Pharmacother* 2020;**126**:109929.
30. Long B, Koyfman A, Gottlieb M. *Lactobacillus reuteri* for treatment of infant colic. *Acad Emerg Med* 2020;**27**:1059−60.
31. Lee Y, Sugihara K, Gillilland MG, Jon S, Kamada N, Moon JJ. Hyaluronic acid-bilirubin nanomedicine for targeted modulation of dysregulated intestinal barrier, microbiome and immune responses in colitis. *Nat Mater* 2020;**19**:118−26.
32. Liu Y, Cheng Y, Zhang H, Zhou M, Yu Y, Lin S, et al. Integrated cascade nanozyme catalyzes *in vivo* ROS scavenging for anti-inflammatory therapy. *Sci Adv* 2020;**6**:eabb2695.
33. Wirtz S, Neufert C, Weigmann B, Neurath MF. Chemically induced mouse models of intestinal inflammation. *Nat Prot* 2007;**2**:541−6.
34. Lee JY, Cevallos SA, Byndloss MX, Tiffany CR, Olsan EE, Butler BP, et al. High-fat diet and antibiotics cooperatively impair mitochondrial bioenergetics to trigger dysbiosis that exacerbates pre-inflammatory bowel disease. *Cell Host Microbe* 2020;**28**:273−84.
35. Yin CM, Qiao X, Fan XZ, Chen ZY, Yao F, Shi DF. Differences of gut microbiota composition in mice supplied with polysaccharides from γ-irradiated and non-irradiated *Schizophyllum commune*. *Food Res Int* 2022;**151**:110855.
36. Liu JJ, Dong W, Zhao J, Wu JQ, Xia JQ, Xie SF, et al. Gut microbiota profiling variated during colorectal cancer development in mouse. *BMC Genom* 2022;**23**:848.
37. Lee CK, Oh SJ, Kim HJ, Kim BH, Kim BK, Park YK, et al. P919 Gut microbial signature and phenotype-specific indicators in fecal microbiota of Korean patients with inflammatory bowel disease. *J Crohn Colitis* 2023;**17**:1028.
38. Dejanovic D, Zhao S, Cruise MW, Bhilocha S, Schirbel A, West GA, et al. 626-Selective deletion of MYD88 signaling in α-SMA positive cells ameliorates experimental intestinal fibrosis *via* posttranscriptional regulation. *Gastroenterology* 2018;**154**: 130−1.
39. Prados ME, Garcia-Martin A, Unciti-Broceta JD, Palomares B, Collado JA, Minassi A, et al. Betulinic acid hydroxamate prevents colonic inflammation and fibrosis in murine models of inflammatory bowel disease. *Acta Pharm Sin B* 2021;**42**:1124−38.